25th ABCM International Congress of Mechanical Engineering
October 20-25, 2019, Uberlândia, MG, Brazil

COB-2019-1872
LIFT AND DRAG CORRELATIONS FOR AN HYDROFOIL ARRAY THROUGH NUMERICAL SIMULATION ANALYSIS.

Luan Cavalari Labigalini
Ricardo de Vasconcelos Salvo
Rafael Sene de Lima
Ismael de Marchi Neto
Rodrigo Corrêa da Silva
Mechanical Engineering Department, Federal University of Technology – Paraná (UTFPR – Campus Londrina), Estrada dos Pioneiros, 3131, Londrina, Paraná.
luanclabigalini@gmail.com

Abstract. *Energy demand is continuously increasing and therewith the greenhouse emissions amount. One viable alternative is based on the investment in renewable energy sources. Even it corresponding to about 14% of global matrix this percentage should still increase in near future, reducing the importance of consolidated sources such as coal and oil. Aiming in hydropower utilization this paper is the first of a series concerning hydrokinetic turbines development. In this first approach the main objective is to investigate lift and drag coefficients over a hydrofoil array, and then, find useful correlations for hydrokinetic turbines. Steady and unsteady two-dimensional numerical simulations of the flow around a NACA4412 profile were performed, and the k-ω SST turbulence model was adopted. Several configurations involving different angle of attack and distance between subsequent profiles were analyzed.*

Keywords: *renewable energy, hydrokinetic turbines, NACA 4412, CFD*

1. INTRODUCTION

The fight against climate change in conjunction with worldwide population growth is one of the most important concerns for humanity at 21st century. As reported by Siirola (2014), in 2011, the 7.01 billion people around the world (OWD, 2017) were supplied by 550 exajoules of energy. In comparison, at 2016, according to IEA (2018), the energy demand grew 4.73%. At the same period, humanity was 7.43 billion people already, presenting approximately 6% rise. Thus, the current population growth rate is higher than current energy demand rate. However, this difference was not carried out cleanly, once carbon dioxide emissions have just intensified (IEA, 2018). Despite of carbon atoms follow a natural cycle, it is unbalanced (Siirola 2014). Carbon emission rate is overreaching carbon dissolution rate into ocean. And the more carbon dioxide at atmosphere exist, the worse consequences are over weather. Therefore, such governance, policies, and treaties are being made in order to not only fulfill an increasing global energy demand with sustainable effort, but also to reduce fossil gas discharge, as detailed by Bracken et al. (2014).

The Sustainable Development Goals (SDGs) for 2030 adopted by global community in 2015 pointed, in its fourth report "*Tracking SDG7: The Energy Progress Report*", major goals for energy of which stand out: Goal 7.1 relating to energy access, Goal 7.2 for an increase in the share of energy consumption from renewable sources and Goal 7.3 which aims the rate of improvement of energy efficiency globally. SDG7 shows that almost 13% of world's population (roughly one billion people) live without access to electricity. Most of these live in underdeveloped countries in Sub-Saharan Africa and Central and Southern Asia. It must be kept in mind that even in countries where universal access to electricity was achieved between 2010 and 2016 (SDG7), i.e. Brazil, still have large areas where part of their population does not have access to electricity. Size, territorial extension of 8.515 million square kilometres, according to the Brazilian Institute of Geography and Statistics (IBGE) and local terrain also make it difficult to transmit energy. Thus, several local communities use sets of motor-generators to locally produce electricity. This kind of generation also plays a role in fossil gas emission (Ardizzon et al., 2014), though it has many origins. In this way, SDG7 Goal 7.2 clearly demonstrates concern about the emission of greenhouse gases and climate change.

Hence, renewable energy resources are shown as trustworthy solution and have been increased its percentage on global energy matrix, mainly biomass, hydropower, solar and wind. Despite they represent almost 20% of energy supply in the world by 2016, it is stood out that from 2011 solar photovoltaic grew its production by nearly 420% (63, 170 to 328,038 GWh), wind by approximately 120 % (436,010 to 957,694 GWh) and hydro, more consolidated, around 16% (3,597,861 to 4,170,035 GWh), which has as main producer the Rep. of China, a global potency (IEA, 2018). Also, this kind of source is famous by hydroelectric, whose dams provide potential energy and can produce huge

amount of energy. However, its environmental harm can be countless regarding the impoundment (Kaunda et al., 2014). But this source is unrestricted nowadays and many and well used forms of exploit kinetic energy from marine currents and rivers are being developed. Moreover, energy grid does not have enough conditions to be spread all over a territory, and some far areas are misused. On this matter, hydrokinetic turbine is a focus of such researches, once its low free-stream velocity operation and high energy density can result in a small turbine, which its production can comply few families and reach remote areas, as was detailed by Vermaak et al. (2014). Similar approaches were made recently by many researches: Riglin et al. (2016) and Schleicher et al. (2015) designed a hydrokinetic turbine almost identical to Kaplan type, while Wang et al. (2019) designed one comparable to wind turbines.

In order to achieve better efficiencies, this paper analyses the flow over a hydrofoil array, commonly seen in tidal turbines. The main aim is to find correlations for lift and drag, with a variety of distances of separation between blades and their angles of attack. A less expensive way to do it is through numerical simulation, also known as Computational Fluid Dynamics (CFD). As reported by Ardizzon et al. (2014), CFD is a useful tool on realistic analysis and predictions over turbomachinery operation, becoming the state-of-art in this kind of projects.

2. METHODOLOGY

The study requires prior selection of the airfoil profiles as described in section 2.1. After selection, mesh independence tests are performed for a single profile by comparison of lift and drag for different angle of attack with experimental data. Only after the appropriated mesh, boundary conditions and simulation parameters are obtained for an isolated hydrofoil the hydrofoil array is addressed. The hydrofoil array configuration analysis methodology follows the one proposed by Cebrián et al. (2013) and is presented in section 2.2. By the end, correlations between relative angles, lift and drag, at different distances – in terms of solidity - and angles of attack could be found.

2.1 Airfoil profile selection

As blades from turbines, the profiles should be suitable for energy transference from the flow as much as possible (Halder et al., 2017). Nevertheless, this transmittal may damage blade structure if pressure over-decreases. It means that not only lift force, but also cavitation are shown as the most important coefficients for power generation, and according to preceding researches the most indicated profiles for hydrokinetic turbines are NACA 0015 (Halder et al., 2017), NACA 4412 (Wang et al., 2019), Abuan and Howell (2019) treat NACA 4415, NACA 4418 and NACA 4424, and NACA 6412 (Hoghooghi et al., 2018). In the current work the NACA 4412 data is analyzed.

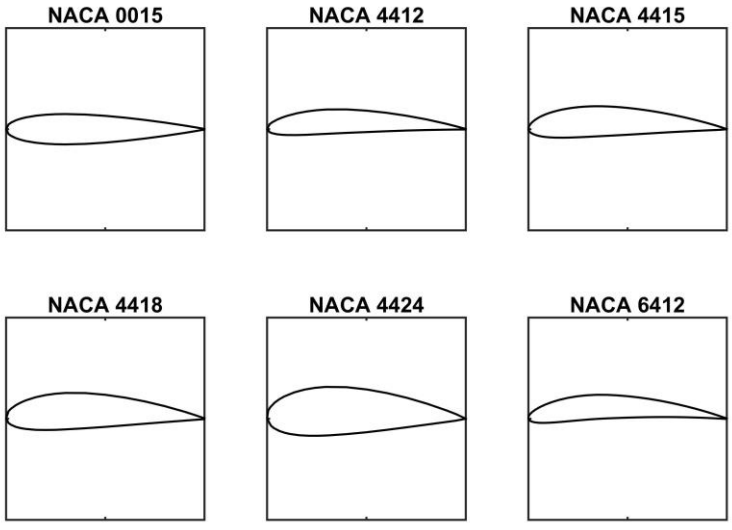

Figure 1. Different NACA profiles studied in previous researches.

2.2 Numerical Simulation

Firstly, with the imported profile points the mesh could be generated using ANSYS ICEM software and a chord equal to 1 m was assumed. A C-Grid domain with a diameter of 100 times the chord was established, and three different two-dimensional meshes were created, with hexahedral elements and following a Y+ rule as 1. Their respective number of cells can be seen on Tab. 1, and a visualization of elements in Fig. 2.

Table 1. Meshing names and their respective number of elements.

Mesh	Number of elements
Mesh A	174,500
Mesh B	375,000
Mesh C	480,000

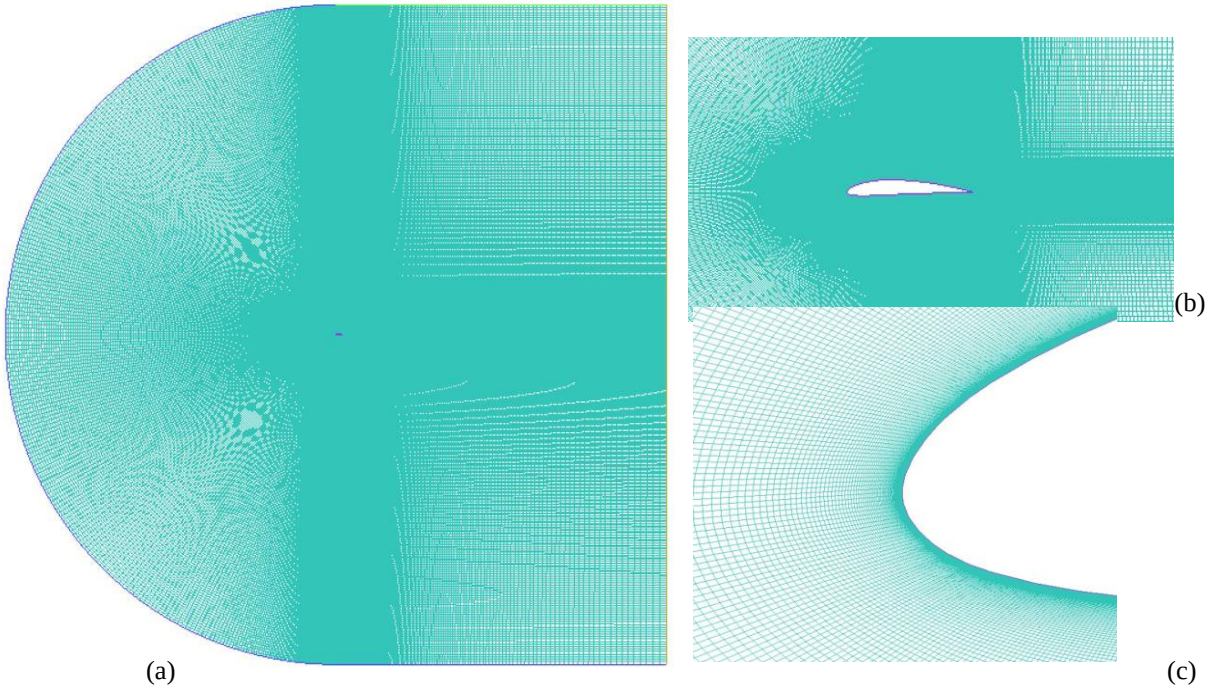

Figure 2. Mesh B domain (a) and zoom around NACA profile (b) and (c).

Secondly, for mesh independence analyses, 15 simulations were performed for the NACA4412 isolated profile and the results compared to experimental data, shown in section 3.1. Software ANSYS Fluent was chosen for the simulations. The fluid phase was treated as water with constant density 998.2 kg/m³ and viscosity 1.003 x 10^{-3} kg/m.s. An uniform velocity profile (U_{in}) was prescribed at the inlet yielding a Reynolds number, based on the cord length, of 1.64E06. At outlet the static pressure was prescribed as 0 [Pa]. Due to boundary layer separation, especially at high attack angles, obtaining convergence in steady state simulations may be difficult. Thus, in this work all simulations where steady convergence was not obtained were continued in an unsteady manner. The time step was set as 1E-3 s, and a total physical time of 20 s was simulated for each case. This total time has proven to be more than sufficient for flow development and the stabilization of Drag and Lift coefficients. For turbulence modeling the k-ω SST model was adopted, which is the same model used by Javadi and Nilsson (2017), Schleicher et al. (2015), Halder et al. (2017), Tian et al. (2016) and Cebrián et al. (2013). The pressure velocity coupling was accomplished with SIMPLE scheme and second order upwind was chosen for spatial interpolation while the First Order Implicit scheme was adopted for time advancement. Residuals were set to 1E-05 in unsteady and 1E-06 in steady regime, for all equations.

Thirdly, as long as mesh independence was achieved, new computational domains were made and a periodic condition was applied in order to emulate the blade array configuration. New meshes were created following solidity correlation, Eq. (1), in which distances vary according to chord length, see Fig. 3.

$$\sigma = \frac{c}{s} \tag{1}$$

Where c is chord length and s is distance between profiles. Solidities values evaluated were 0.50, 0.63, 0.77, 1.00 1.43 and 2.50. A fixed distance before and after the hydrofoil, which allowed flow and wake vortex develop was adopted. The boundary conditions, turbulence model, numerical methods and residuals used were the same as previous. Turbulence parameters were set as 0.0074 and 0.389 for turbulent kinetic energy (k) and specific dissipation rate (ω), respectively, according to results obtained by Cebrián et al. (2013)

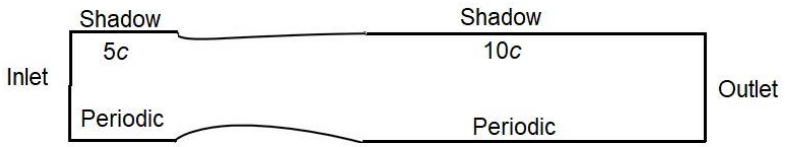

Figure 3. Domain schematic, with distances and boundary conditions used.

Lastly, correlations of lift and drag coefficients as a function of angle of attack and solidity were found.

3. RESULTS

3.1 Mesh Independence Test

Mesh independence is verified through comparison of numerical obtained lift and drag coefficients with experimental data from Wadcock (1987). Numerical coefficients, experimental data and the difference between then are shown in Tab. 2. It was noted that for higher angles of attack convergence is a tough task to achieve concerning a steady-state simulation. Therefore, the studied case has shown to be intrinsically unsteady, and this model must be deemed. From Table 2 it may be understood that Mesh B is fine enough for the proposed simulation. Considering the geometric similarity between the cases - isolated hydrofoil and hydrofoils array, when the artifice of periodic boundary conditions is considered, the authors opted to use a similar mesh (same number of elements and Y+ requirements) for the remaining simulations.

Table 2. Independence mesh analysis of NACA 4412 simulation, according to drag and lift coefficient results, compared to experimental data (Wadcock, 1987).

Mesh	Drag / Lift	Experimental Data	Difference (%)
0°			
Mesh A	0.0022653 / 0.34664	0.005675 / 0.46794	60.08 / 25.92
Mesh B	0.012566 / 0.42362		121.43 / 9.47
Mesh C	0.012575 / 0.42367		121.59 / 9.46
10°			
Mesh A	0.020613 / 1.2746	0.025058 / 1.36042	17.74 / 6.31
Mesh B	0.025694 / 1.38660		2.54 / 1.92
Mesh C	0.026266 / 1.38500		4.82 / 1.81
15°			
Mesh A	0,036804 / 1,61170	0.090543 / 1.22170	59.35 / 31.92
Mesh B	0.048651 / 1.61510		46.27 / 32.20
Mesh C	0.048351 / 1.61970		46.60 / 32.58

Then, for a precisely analysis, other angles of attack were performed with the validated mesh, as can be seen in Fig. 4, where it is possible to observe that the simulations results are very close to the experimental data in the range 0°-12°, from this value on the results begin to distance themselves from the experimental data, indicating that the simulations postponed the stall. As the angle of attack increases, the boundary layer detachment point moves toward the leading edge, thus increasing the size of the viscous wake. Along with the wake the three-dimensional effects also increase. Thus, when performing two-dimensional simulations of airfoil/hydrofoil profiles, any results obtained at angles of attack close to or greater than the stall angle must be treated with the utmost caution. This was already expected, i.e. recently reported by Matyuschenko et al. (2017). Despite the difference between experimental data and numerical results, it can be seen that physical behavior is preserved: lift improvement until stall and drag growth limitless. Therefore, away from stall region, single profile results are assumed as validated and taken as a guarantee for validity of incoming analysis.

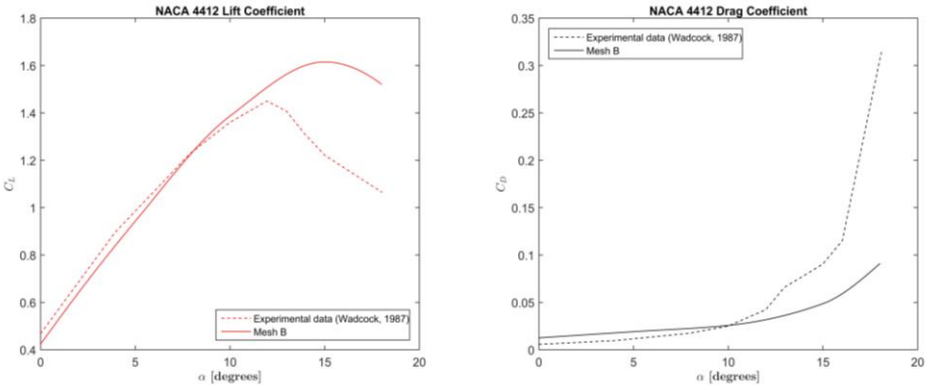

Figure 4. Lift and Drag comparison between Mesh B results from validation process and experimental data (Wadcock, 1987).

3.2 Array correlations

For single hydrofoil solidity was assumed as 0, once *s* tends to ∞. The results are detailed in Tab. 3 and 4, and summarized in Fig. 5.

Table 3. Lift Coefficient obtained for different angles of attack (AoA) and distances between profiles, in terms of solidity.

AoA	Solidity						
	0.00	0.50	0.63	0.77	1.00	1.43	2.50
0°	0.42362	0.24806	0.22723	0.20814	0.18422	0.15480	0.11528
5°	0.94283	0.51679	0.47098	0.41439	0.37421	0.22127	0.11099
10°	1.38660	0.77143	0.68315	0.61022	0.53824	0.41560	0.14900
15°	1.61510	1.01421	0.88744	0.79771	0.68719	0.52788	0.18124
18°	1.52110	1.11740	0.99540	0.89629	0.77879	0.59895	0.22092
20°	1.35720	1.16108	1.05368	0.95048	0.81242	0.64122	0.29598

Table 4. Drag Coefficient obtained according to different angles of attack (AoA) and distances, in terms of solidity.

AoA	Solidity						
	0.00	0.50	0.63	0.77	1.00	1.43	2.50
0°	0.012566	0.021702	0.022052	0.022318	0.021932	0.022408	0.024468
5°	0.019081	0.048234	0.048073	0.047012	0.044818	0.039982	0.034458
10°	0.025694	0.090538	0.088494	0.084855	0.087340	0.069315	0.049102
15°	0.048651	0.144293	0.142658	0.135247	0.124575	0.106311	0.068206
18°	0.090802	0.178183	0.177142	0.168746	0.155250	0.131221	0.085284
20°	0.094124	0.199129	0.199759	0.190954	0.177646	0.148567	0.103498

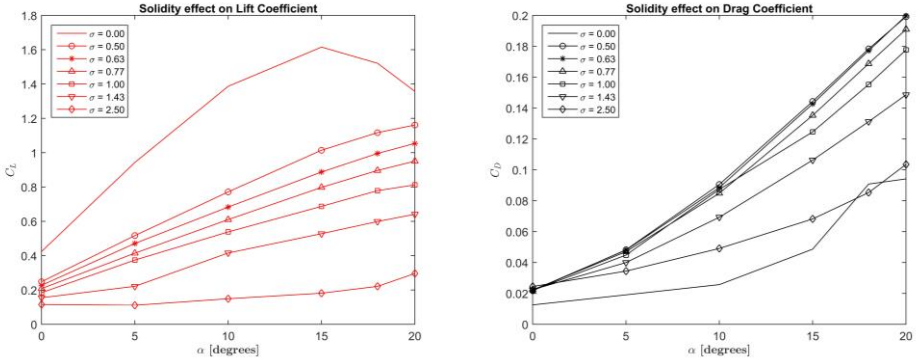

Figure 5. Lift and Drag functions in respect of angles of attack, for different solidities values.

As shown in Fig. 5, solidity is critical in the profile performance. Lift coefficient monotonically increases with distance between hydrofoils while drag coefficient has a more complicated relation: for solidity values between 0 and 0.5 drag coefficient increases and then as solidity increases beyond 0.5 drag coefficient stats to decrease - except when solidity equals one.

The proximity between profiles contracts the free stream increasing the favorable pressure gradient, which accelerates the flow - seen in Fig. 7. Therefore, the flow within boundary layer has more energy allowing it to resist the adverse pressure gradient for a longer distance, delaying the boundary layer separation – same behavior reported by Cebrián et al. (2013). Thus, stall has not been reached in any tested arrangement. Furthermore, that tendency is clearly visualized in Fig. 8 (a), which has shown comparison between wall shear stress for a single hydrofoil and an array with solidity equals to 2.50, at an angle of attack of 20°. It is noticed the existence of boundary layer separation only for an isolated profile, once for solidity 2.50 wall shear stress values are exclusively positive. That behavior can also be seen in Fig. 9. In other words, at this moment, the interaction between blades prevails over flow development.

Unlike one might expect, lift coefficient also decreases in this case when compared to a single hydrofoil. This is due to the fact that flow accelerates not only on the upper surface but also under the profile, resulting in a smaller net pressure difference between the upper and lower profile surfaces. That is reported in Fig. 8 (b), where pressure coefficients are quite smaller for a higher solidity value. A more general view is provided in Fig. 10 with the visualization of how pressure field change. In other hand, single hydrofoils flow's can develop at an enough high angle of attack, once its energy is not sufficient against adverse pressure level, and the recirculation zone on trailing edge increases, as can be seen in Fig. 11, where turbulence kinetic energy is intensified.

Due to stall delay, further numerical simulations will be necessary in order to find correlations for optimum relative angles.

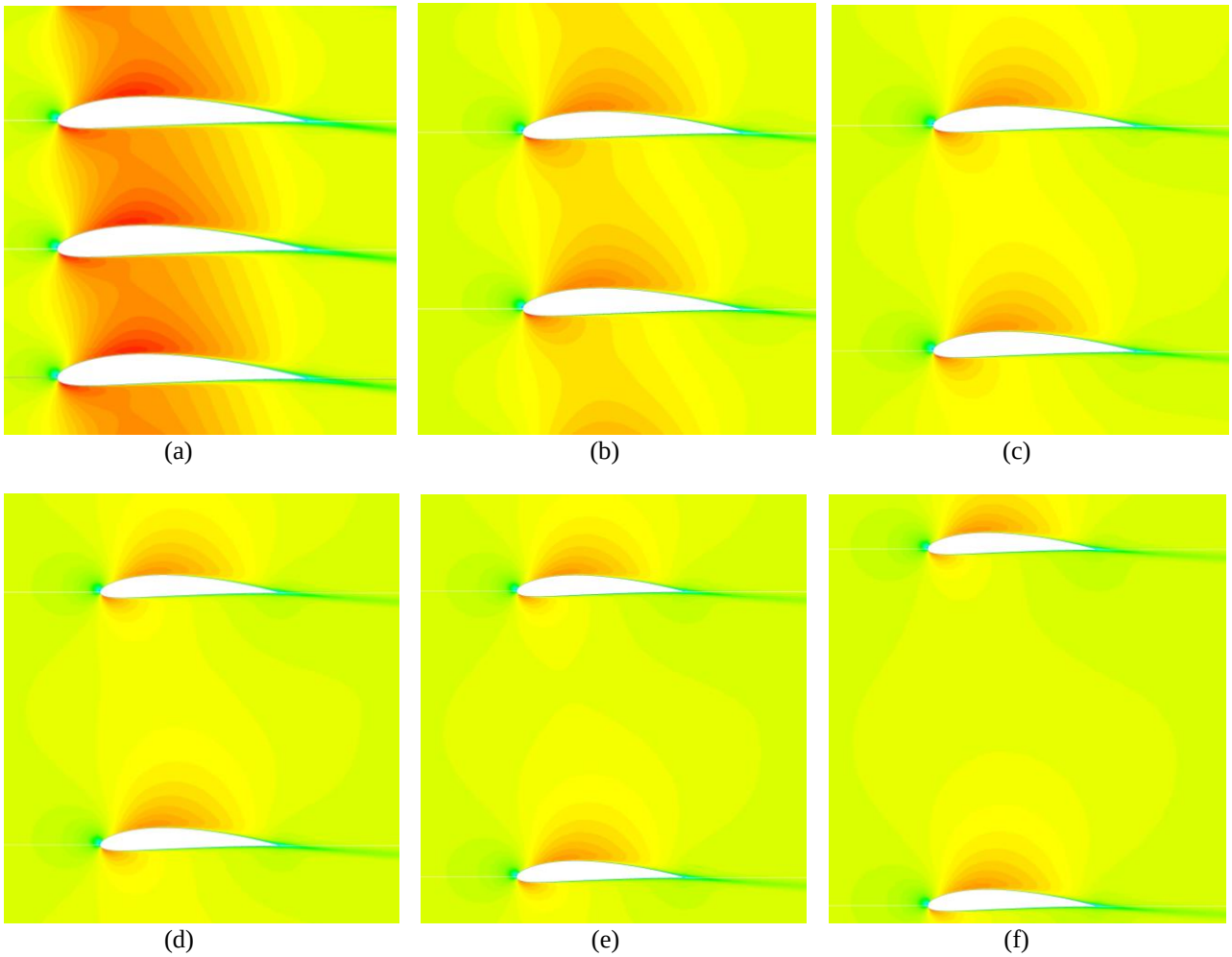

Figure 7. Velocity fields at an angle of attack equals to 0°, from solidity (a) 2.50 until (f) 0.5. All contours have same specified maximum and minimum velocities.

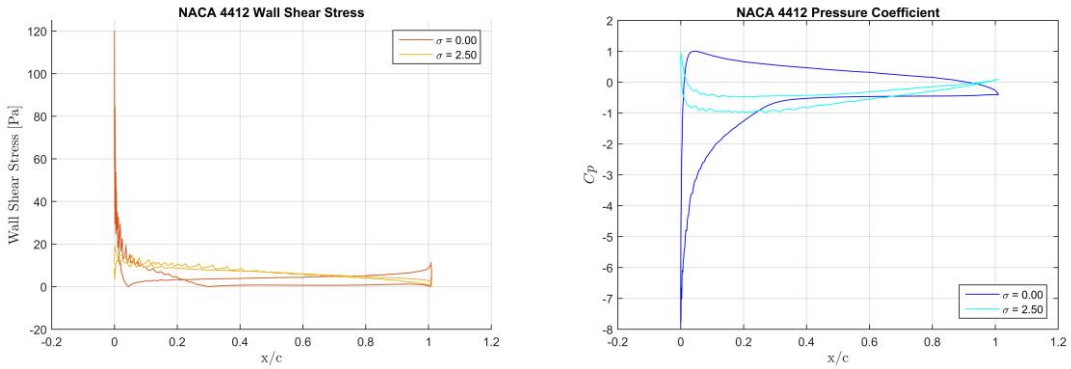

(a) (b)

Figure 8. Comparison between solidities 0 and 2.50 for an angle of attack equals to 20°. (a) Wall shear stress. (b) Pressure Coefficient.

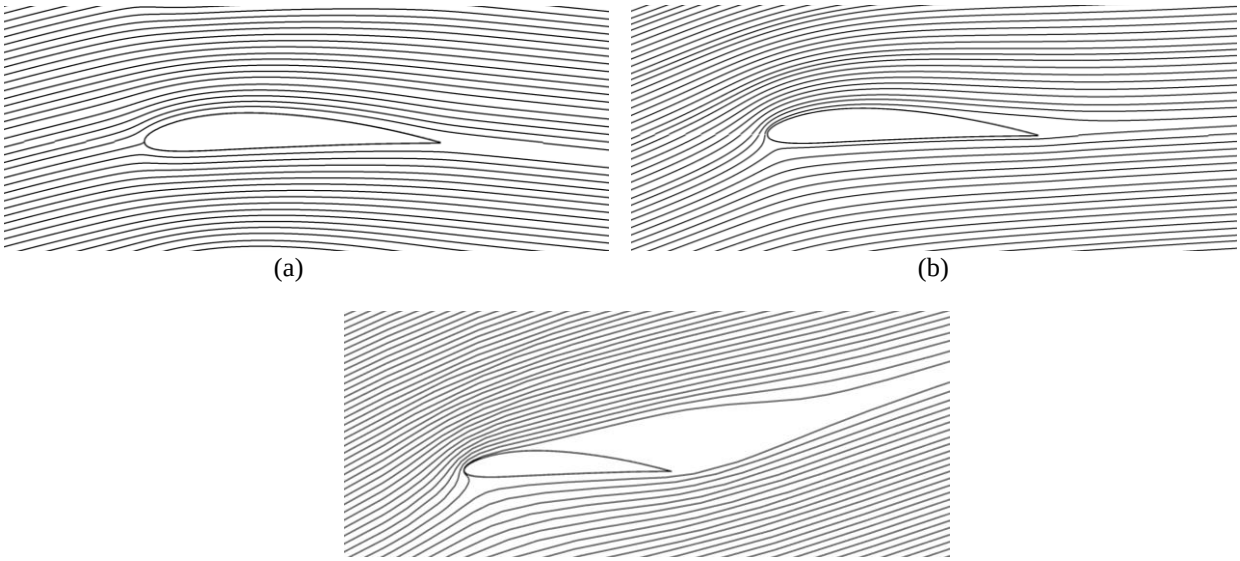

(a) (b)

(c)

Figure 9. Velocity streamlines at an angle of attack equals to 0°, from solidity (a) 2.50, (b) 0.50 and (c) 0.

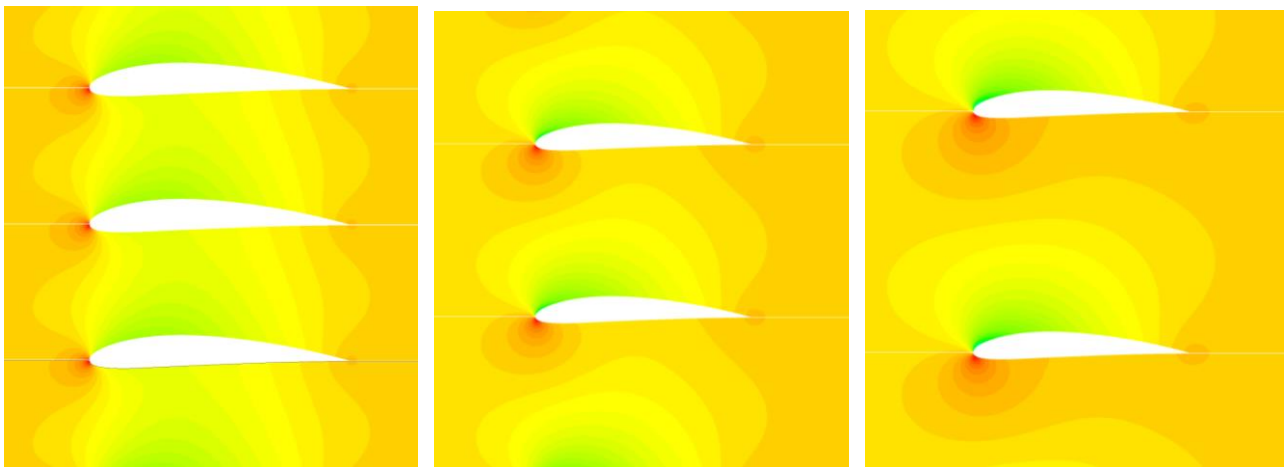

(a) (b) (c)

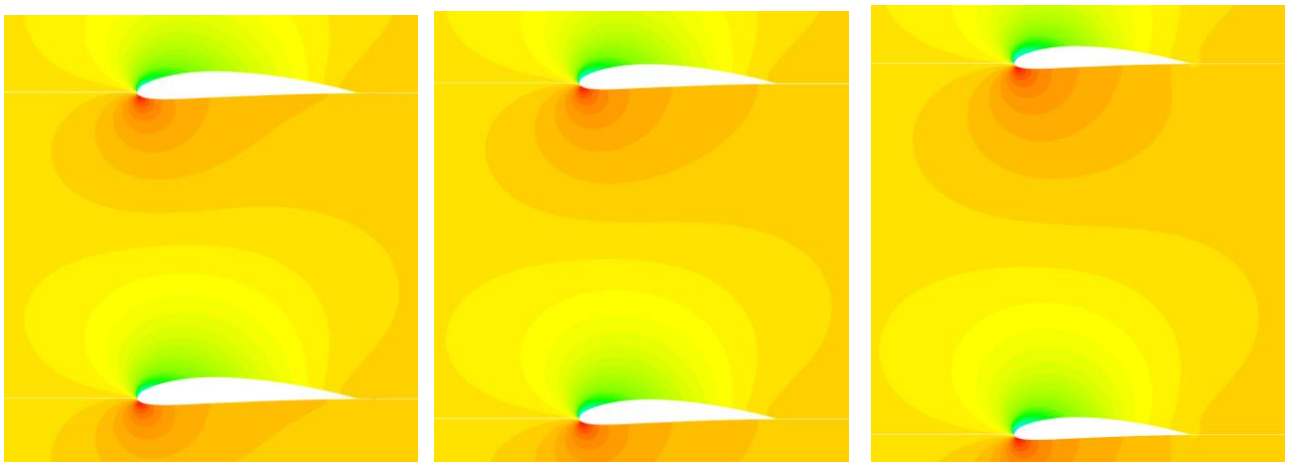

(d) (e) (f)

Figure 10. Pressure fields at an angle of attack equals to 20°, from solidity (a) 2.50 until (f) 0.50. All contours have same specified maximum and minimum velocities.

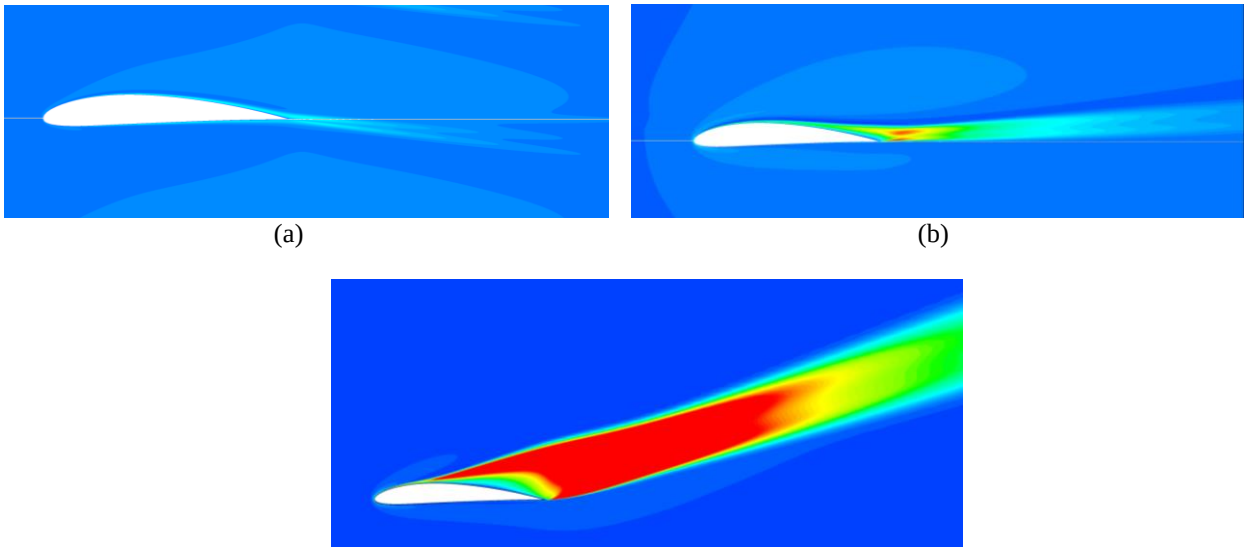

(a) (b)

(c)

Figure 11. Turbulent kinetic energy field at an angle of attack equals to 20°, from solidity (a) 2.50, (b) 0.50 and (c) 0. All contours have same specified parameters – array arrangement took as reference.

The aim of this study is focused on a relationship between the coefficients and solidities, separated by angles of attack. As a single profile tends to zero solidity value - distance tends to infinity -, its coefficient values represent an asymptotic function. Thus, it may be assumed that fitter correlations between the coefficients and solidity could be in power function form, similarly as Cebrián et al. (2013) has done, or in rational form. Curve Fitting MATLAB Toolbox was used for this task, and results are shown in Tab. 6 and 7.

Table 6. Results of Drag Coefficient regression according to different angles of attack (AoA), in function of solidity.

Drag Coefficient		
AoA	Function	R-Square
0°	(19.99*σ + 2.147) / (σ ^2 + 787*σ + 174)	0.9651
5°	(0.1259*σ + 0.009292) / (σ ^2 + 1.525*σ + 0.4872)	0.9997
10°	(0.1046*σ + 0.0157) / (σ ^2 - 0.1608*σ + 0.606)	0.9811
15°	(0.1475*σ + 0.02487) / (σ ^2 – 0.1332*σ + 0.5094)	0.9826
18°	(0.1598*σ + 0.06523) / (σ ^2 – 0.2817*σ + 0.7158)	0.9811
20°	(0.2048*σ + 0.06444) / (σ ^2 – 0.1749*σ + 0.683)	0.9903

Table 7. Results of Lift Coefficient regression according to different angles of attack (AoA), in function of solidity.

Lift Coefficient		
AoA	Function	R-Square
0°	0.4237 – 0.2351*σ^(0.3878)	0.9988
5°	0.9422 - 0.5901*σ^(0.4903)	0.9985
10°	1.385 - 0.856*σ^(0.4799)	0.9925
15°	1.613 - 0.9222*σ^(0.5899)	0.9922
18°	1.518 – 0.7277*σ^(0.7823)	0.9915
20°	1.363 - 0.5073*σ^(1.056)	0.9910

Drag results regression shown to be a hard task, according to R-square values, and lift values could be well approximated, as can be visualized in Fig. 12, though. Once that is a simplified two-dimensional case, the main reason of unfitness may be the values disagreement originated by three-dimensional accuracy loses, which is an inherent characteristic of drag forces.

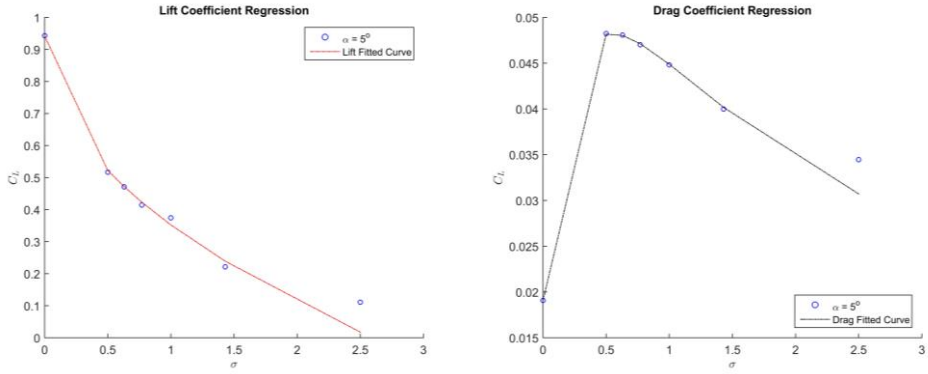

Figure 12. Lift and Drag plot of their regression functions in respect of solidity, for an angle of attack equals to 5°.

Despite difficulty to find relationship between coefficients and angles of attack, these correlations are well seen, even as approximations. It is an easy way to predict blades performance in different distances, opening design possibilities, which may be exploited in further researches. These simulations were based and compared with respective single profile CFD simulation. Real application can differ in many forms - specially stall angle, for example - and a possible further experimental validation can be developed. But it is presented as irrefutable how profile coefficients are dependent of their arrangement.

4. ACKNOWLEDGEMENTS

Authors would like to thanks the Federal University of Technology - Paraná for financial support and the company WEG Electric Equipment SA, for allowing their computers and ANSYS License to be used, in order to promote knowledge development.

5. REFERENCES

Abuan, B.E., Howell, R.J., 2019. "The performance and hydrodynamics in unsteady flow of a horizontal axis tidal Turbine". *Renewable Energy*, Vol. 133, pp. 1338-1351.

Ardizzon, G., Cavazzini, G., Pavesi, G., 2014. "A new generation of small hydro and pumped-hydro power plants Advances and future challenges". *Renewable and Sustainable Energy Reviews*, Vol. 31, pp. 746–761.

Bracken, L.J., Bulkeley, H.A., Maynard, C.M., 2014. "Micro-hydro power in the UK: The role of communities in an emerging energy resource". *Energy Policy*, Vol. 68, pp. 92-101.

Cebrián, D., Ortega-Casanova, J., and Fernandez-Feria, R., 2013. "Lift and drag characteristics of a cascade of flat plates in a configuration of interest for a tidal current energy converter: Numerical simulations analysis". *Journal of Renewable and Sustainable Energy*, Vol. 5, Issue 4, pp. 1–20.

Halder, P., Rhee, S. H., Samad, A., 2017. "Numerical optimization of Wells turbine for wave energy extraction". *International Journal of Naval Architecture and Ocean Engineering*, Vol. 9, Issue 1, pp. 11-24.

Hoghooghi, H., Durali, M., Kashef, A., 2018. "A new low-cost swirler for axial micro hydro turbines of low head potential". *Renewable Energy*, Vol. 128, Part A, pp. 375-390.

IEA, 2018. "Key World Energy Statistics 2018", International Energy Association. 21 Feb. 2019 <https://www.iea.org>.

Javadi, A., Nilsson, H., 2017. "Detailed numerical investigation of a Kaplan turbine with rotor-stator interaction using turbulence-resolving simulation". *International Journal of Heat and Fluid Flow*, Vol. 63, pp. 1-13.

Kaunda, C.S., Kimambo, C.Z., Nielsen, T.K., 2014. "A technical discussion on microhydropower technology and its turbines". *Renewable and Sustainable Energy Reviews*, Vol. 35, pp. 445-459.

Matyuschenko, A. A., Kotov, E. V., Garbaruk, A. V., 2017. "Calculations of flow around airfoils using two-dimensional RANS: an analysis of the reduction in accuracy". *St. Petersburg Polytechnical University Journal: Physics and Mathematics*, Vol. 3, pp. 15-21.

OWD, 2017. "World Population Growth" Our World in Data. 23 Feb. 2019 <https://ourworldindata.org>.

Riglin, J.D., Carter III, F., Oblas, N., Chris Schleicher, W., Daskiran, C., Oztekin, A., 2016. "Experimental and numerical characterization of a full-scale portable hydrokinetic turbine prototype for river applications". *Renewable Energy*, Vol. 99, pp. 772-778.

Schleicher, W.C., Riglin, J.D., Oztekin, A., 2015. "Numerical characterization of a preliminary portable micro-hydrokinetic turbine rotor design". *Renewable Energy*, Vol. 76, pp. 234-241.

Siirola, J.J., 2014. "Speculations on global energy demand and supply going forward". *Current Opinion in Chemical Engineering*, Vol. 5, pp. 96-100.

Tian, W., Song, B., VanZwieten, J. H., Pyakurel, P., Li, Y., 2016. "Numerical simulations of a horizontal axis water turbine designed for underwater mooring platforms". *International Journal of Naval Architecture and Ocean Engineering*, Vol. 8, Issue 1, pp. 73-82.

Vermaak, H.J., Kusakana, K., Koko, S.P., 2014. "Status of micro-hydrokinetic river technology in rural applications: A review of literature". *Renewable and Sustainable Energy Reviews*, Vol. 29, pp. 625-633.

Wadcock, A. J., 1987. "Investigation of low-speed turbulent separated flow around airfoils (Analytical Methods)" *NASA Contractor Report*.

Wang, W., Yin, R., Yan, Y., 2019. "Design and prediction hydrodynamic performance of horizontal axis micro-hydrokinetic river turbine". *Renewable Energy*, Vol. 133, pp. 91-102.

6. RESPONSIBILITY NOTICE

The authors are the only responsible for the printed material included in this paper